



POTSDAM-INSTITUT FÜR
KLIMAFOLGENFORSCHUNG

Originally published as:








Irankhah, R., Mehrabbeik, M., Parastesh, F., Rajagopal, K., Jafari, S., [Kurths, J.](#) (2024): Synchronization enhancement subjected to adaptive blinking coupling. - Chaos, 34, 2, 023120.

DOI: <https://doi.org/10.1063/5.0188366>

RESEARCH ARTICLE | FEBRUARY 20 2024

Synchronization enhancement subjected to adaptive blinking coupling

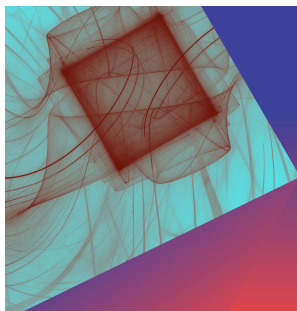
Special Collection: [Advances in Adaptive Dynamical Networks](#)

Reza Irankhah ; Mahtab Mehrabbeik ; Fatemeh Parastesh ; Karthikeyan Rajagopal ;
Sajad Jafari  ; Jürgen Kurths 



Chaos 34, 023120 (2024)

<https://doi.org/10.1063/5.0188366>



Chaos: An Interdisciplinary Journal of Nonlinear Science

Focus Issue:

From Sand to Shrimps: In honor of Jason A.C. Gallas

Guest Editors: Marcus W. Beims, Thorsten Pöschel, Pedro G. Lind

[Submit Today!](#)

Synchronization enhancement subjected to adaptive blinking coupling

Cite as: Chaos 34, 023120 (2024); doi: 10.1063/5.0188366

Submitted: 21 November 2023 · Accepted: 25 January 2024 ·

Published Online: 20 February 2024



View Online



Export Citation



CrossMark

Reza Irankhah,¹ Mahtab Mehrabbeik,¹ Fatemeh Parastesh,² Karthikeyan Rajagopal,² Sajad Jafari,^{1,3,a)} and Jürgen Kurths^{4,5}

AFFILIATIONS

¹Department of Biomedical Engineering, Amirkabir University of Technology (Tehran Polytechnic), Tehran 159163-4311, Iran

²Centre for Nonlinear Systems, Chennai Institute of Technology, Chennai 600069, India

³Health Technology Research Institute, Amirkabir University of Technology (Tehran Polytechnic), Tehran 159163-4311, Iran

⁴Potsdam Institute for Climate Impact Research, Potsdam 14473, Germany

⁵Institute of Physics, Humboldt University of Berlin, Berlin 12489, Germany

Note: This paper is part of the Focus Issue on Advances in Adaptive Dynamical Networks.

^{a)}Author to whom correspondence should be addressed: sajadjafari83@gmail.com

ABSTRACT

Synchronization holds a significant role, notably within chaotic systems, in various contexts where the coordinated behavior of systems plays a pivotal and indispensable role. Hence, many studies have been dedicated to investigating the underlying mechanism of synchronization of chaotic systems. Networks with time-varying coupling, particularly those with blinking coupling, have been proven essential. The reason is that such coupling schemes introduce dynamic variations that enhance adaptability and robustness, making them applicable in various real-world scenarios. This paper introduces a novel adaptive blinking coupling, wherein the coupling adapts dynamically based on the most influential variable exhibiting the most significant average disparity. To ensure an equitable selection of the most effective coupling at each time instance, the average difference of each variable is normalized to the synchronous solution's range. Due to this adaptive coupling selection, synchronization enhancement is expected to be observed. This hypothesis is assessed within networks of identical systems, encompassing Lorenz, Rössler, Chen, Hindmarsh-Rose, forced Duffing, and forced van der Pol systems. The results demonstrated a substantial improvement in synchronization when employing adaptive blinking coupling, particularly when applying the normalization process.

Published under an exclusive license by AIP Publishing. <https://doi.org/10.1063/5.0188366>

Synchronization is a fundamental concept closely linked to the structure of networks, encompassing network topology that defines the connections among nodes and the nature of interactions determined by couplings. Networks can generally be classified as static, evolving, or adaptive. Adaptive networks are considered more realistic models that can emulate manifold real-world phenomena. Previous research has mainly concentrated on the adaptability of network topology to illustrate its influence on synchronization improvement. However, recent attention has shifted toward the adaptability of coupling configurations, which has proven to affect enhancing synchronization significantly. In this study, we explore a novel adaptive blinking network where, at each time step, the single-variable diffusive coupling is determined based on the normalized average nodal difference. Through various examples, we demonstrate that

this structure impacts synchronization by reducing the required coupling strength to attain this state.

I. INTRODUCTION

Complex dynamical networks are characterized by multiple interconnected elements or nodes having temporal dynamical behaviors.¹⁻³ These networks exhibit intricate interconnections and possess the capacity to manifest emergent phenomena.⁴⁻⁶ Complex dynamical networks are found extensively in both natural and technological domains, ranging from the neuronal connections within the human brain⁷ to the complicated web of interactions observed on social media platforms.⁸ They provide a framework for understanding diverse phenomena like information flow,

synchronization, and resilience. Consequently, networks form a fundamental study area in diverse fields. Synchronization is an important phenomenon in complex networks such as biological networks.^{9–11} This state refers to the emergence of coherent and coordinated behavior across the network without centralized control.^{12,13} It can involve complete synchronization,¹² generalized synchronization,¹⁴ phase synchronization,¹⁵ lag synchronization,¹⁶ and partial synchronization, such as cluster synchronization¹⁷ and chimera.² Examples include the synchronization of neural firing in the brain,^{18,19} alignment of circadian rhythms,^{20,21} oscillations of power grids,²² and spreading opinions in social networks.²³ Synchronization arises from interaction between network components and can be modeled using dynamical systems theory.

The impact of network topology on the synchronization in complex networks has been the subject of extensive research. Connectivity structure and coupling frameworks are key factors influencing synchronization.^{24,25} Various studies have explored this relationship, such as research by Hong *et al.*²⁶ and Wu *et al.*²⁷ investigating synchronization in small-world networks. Wang and Chen²⁸ and Moreno and Pacheco²⁹ focused on synchronization dynamics in scale-free networks. Given the practical importance of synchronization, efforts have also been directed toward improving synchronization in networks with static^{30–32} or temporal evolving structures^{33–35} and adaptive ones.^{36–38}

In a broad context, adaptive networks can be described as dynamic networks that continuously reconfigure their structure according to predetermined rules influenced by the dynamical states of their nodes.^{39,40} For instance, Zhou and Kurths³⁶ found that the synchronization in weighted scale-free networks can be significantly improved by utilizing a weight adaptation scheme based on the local synchronization of nodes. Within this adaptive framework, the coupling strength between neighboring nodes is progressively enhanced, which leads them to achieve synchronization. Assenza *et al.*³⁷ presented a simple model for adaptive networks of phase oscillators, wherein the links connected to each node were weighted according to the cumulative incoming strength and the local synchronization level. The presented mechanism was based on the notion that local synchronization can be enhanced through the interplay of two mechanisms: homophily, which reinforces connections with units exhibiting similar characteristics within the network, and homeostasis, which ensures the stability of the input strength received by each unit. Employing a similar homophily principle, Eom *et al.*³⁸ introduced an adaptive network in which a fitness function controls the network's configuration. This function promotes the connection of oscillators that share more closely aligned phases. They asserted that such adaptivity has the potential to result in improved synchronization and can also lead to percolation.

The studies mentioned above focused on the network topology while keeping the coupling function constant over time. Besides these studies, some researchers have highlighted the impact of time-varying couplings on synchronization. These studies delve into how changes in the coupling mechanisms over time can significantly influence the synchronization behavior of systems. As an illustration, Parastesh *et al.*⁴¹ conducted a study involving a network with blinking coupling, where the variables were involved in the coupling periodically with a certain blinking period. They demonstrated that synchronization stability progressively approaches that of the

average network when the coupling blinks rapidly, following a linear trend. Consequently, synchronization can be enhanced based on the larger Lyapunov exponent of the uncoupled system. In another study, Dayani *et al.*⁴² proposed an optimal time-varying coupling strategy to improve synchronization. This approach considers small time intervals in each of which the coupling is chosen from all potential single-variable couplings based on the smallest local Lyapunov exponent. They assessed the effectiveness of this method by applying it to various networks comprising Rössler, Chen, and Chua systems.

This paper presents a basic contribution in the form of an adaptive blinking network. The uniqueness of this network lies in its dynamic coupling selection mechanism, which is tied to the identification of variables possessing the highest average nodal difference values. This adaptive blinking network marks a departure from traditional approaches by incorporating a nuanced and highly flexible strategy that dynamically adjusts the coupling between nodes based on the distinctive characteristics of nodal differences. Through this inventive approach, the paper opens new avenues for exploring dynamic network behaviors and significantly enhances our understanding of adaptive systems. Section II elaborates on the intricate details of this adaptive coupling scheme. In Sec. III, empirical results on six diverse network examples are provided, which demonstrate significant synchronization enhancement through adaptive blinking coupling. Last, Sec. IV provides a comprehensive discussion and summarizes the paper's key contributions.

II. MODEL AND METHOD

In this study, a novel blinking network, which does not adhere to a predefined time-varying coupling scheme, is introduced. Instead, we consider a scenario where the coupling scheme adaptively switches among the $n \rightarrow n$ configurations (according to the notations in Ref. 43), where $n = 1, \dots, d$, at each time instance t . To start with, considering a network of N interconnected dynamical units within the context of networked dynamical systems, each system's dynamics, denoted as X_i , which is a d -dimensional vector of state variables $x_{i1}, x_{i2}, \dots, x_{id}$, can be expressed as a solution to the following differential equation:

$$\dot{X}_i = F(X_i) - \sigma \sum_{j=1}^N L_{ij} H(t) X_j, \quad (1)$$

where $F(X_i) : R^d \rightarrow R^d$ signifies the intrinsic dynamics of system i , σ is the coupling parameter, $L_{N \times N}$ is the Laplacian matrix ($\sum_{j=1}^N L_{ij} = 0$), and $H(t) : R^d \rightarrow R^d$ is the coupling function at time t .

To dynamically select the coupling configuration, an adaptive approach is employed. Initially, the pairwise nodal difference vectors, denoted as $|X_j - X_i|$ for $i = j = 1, \dots, N$ with $j \neq i$, are computed. Subsequently, the d th variable associated with the highest average difference determines the $d \rightarrow d$ coupling scheme at each time t . This adaptive method ensures that the coupling configuration aligns with the variable exhibiting the most significant difference, thereby adapting to the evolving system dynamics. For the sake of clarity, consider an adaptive blinking network comprising N interconnected identical three-dimensional systems, each represented by $X_i = [x_i, y_i, z_i]^T$. To ascertain the coupling configuration at each time t , the averaged nodal difference vectors, denoted as V_d , can be

computed as follows:

$$\begin{aligned}
 V_d &= \frac{2}{N(N-1)} \left(\sum_{i=1}^{N-1} \sum_{j=i+1}^N |X_j - X_i| \right) \\
 &= \frac{2}{N(N-1)} \left(\sum_{i=1}^{N-1} \sum_{j=i+1}^N |x_j - x_i| \right. \\
 &\quad \left. \times \sum_{i=1}^{N-1} \sum_{j=i+1}^N |y_j - y_i|, \sum_{i=1}^{N-1} \sum_{j=i+1}^N |z_j - z_i| \right). \quad (2)
 \end{aligned}$$

Subsequently, $m = \text{argmax}(V_d)$ represents the variable with the most nodal difference yielding to the most effective coupling. Hence, at each time instance t , the coupling scheme is established as $m \rightarrow m$ coupling [$H_{mm}(t) = 1$]. Here, the notation $n \rightarrow m$ signifies $H_{mn}(t) = 1$, indicating that the disparity in the n th variables of the nodes is incorporated into the m th equation of each respective system.

Upon closer examination of Eq. (2), it becomes evident that the choice of the most effective coupling scheme may be influenced by the domain of the attractor in each dimension, which essentially signifies different scales of the system's variables. To ensure an equitable selection process, the nodal difference vector for each variable is normalized with respect to the attractor range in the synchronization state within the corresponding dimension. This normalization procedure accounts for potential variations in scale across different dimensions and ensures a fair assessment of coupling scheme effectiveness. Accordingly, letting $x_d = x_{\max} - x_{\min}$, $y_d = y_{\max} - y_{\min}$, and $z_d = z_{\max} - z_{\min}$, where indices *max* and *min* refer to the maximum and minimum of the manifold solution, Eq. (2) can be adapted as follows:

$$\begin{aligned}
 V_d &= \frac{2}{N(N-1)} \left(\frac{1}{x_d} \sum_{i=1}^{N-1} \sum_{j=i+1}^N |x_j - x_i|, \frac{1}{y_d} \right. \\
 &\quad \left. \times \sum_{i=1}^{N-1} \sum_{j=i+1}^N |y_j - y_i|, \frac{1}{z_d} \sum_{i=1}^{N-1} \sum_{j=i+1}^N |z_j - z_i| \right). \quad (3)
 \end{aligned}$$

The selection process remains consistent with the previously mentioned approach, where the averaged nodal difference vector V_d dictates the choice of the $d \rightarrow d$ coupling configuration at each time t . It is worth noting that the diffusive characteristic of the coupling function leads to $F(S) = F(X)$, where $S = [x, y, z]$. In the following, we delve into evaluations of network synchronization and highlight the distinctive features of the method in comparison with recently developed blinking networks.

The master stability function (MSF) method provides an analytical mathematical framework for analyzing the stability of the synchronization state within complex networks.⁴⁴ By calculating the eigenvalues of the Jacobian matrix, the MSF helps to determine whether a network's synchronized state is globally stable or susceptible to instabilities. According to the MSF approach, the stability of the synchronous state is tantamount to the stability of the perturbation equation around the zero equilibrium point. Using the

eigenvalues (λ_i) of the Laplacian matrix, the perturbation equation of Network (1) can be defined by the following linearized dynamical equation:

$$\dot{\zeta} = [DF(S) - K_i DH_s(t)] \zeta_i, \quad (4)$$

where $\zeta_i = X_i - S$, S is the synchronous solution, $DF(S) : R^d \rightarrow R^d$ and $DH_s(t) : R^d \rightarrow R^d$ denote Jacobian matrices of $F(X_i)$ and $H(t)$, evaluated at the synchronized state S . Moreover, K is the normalized coupling parameter defined as $K_i = \sigma \lambda_i$, where λ_i is a vector with $\lambda_1 = 0$ and $\lambda_2 \leq \dots \leq \lambda_d$. It is essential to highlight that when applying the definitions mentioned earlier, the coupling functions adhere to linear diffusion, meaning that $DH_s(t) = H(t)$. The presence of a negative sign for the largest Lyapunov exponent indicated as $\Lambda(\lambda_i)$, for $i = 1, \dots, N$, serves as a demonstration of the stability of the synchronization manifold. This stability, in turn, can be interpreted as a fundamental requirement for synchronizing N interconnected oscillators configured in a network topology defined by matrix L .

Upon closer examination of Eq. (4), it can be realized that the coupling scheme represented by $H(t)$ assumes a pivotal role in the synchronization dynamics of N coupled systems. Employing the MSF technique, Huang *et al.*⁴³ investigated the synchronization of renowned low-dimensional systems, exploring all conceivable linear diffusive coupling schemes while maintaining the constancy of $H(t)$ across the run time T . The investigation of time-varying coupling functions, often called blinking coupling, constituted the focal point of the research conducted by Parastesh *et al.*⁴¹ In this study, it was postulated that $H(t)$ transits between the $1 \rightarrow 1$ and $2 \rightarrow 2$ and $3 \rightarrow 3$ coupling schemes periodically with a time period of τ . They employed the MSF method as a result of the coupling's predictable switching pattern. In accordance with the findings presented in Ref. 41 when sufficiently rapid blinking is considered, wherein the blinking period τ takes values considerably shorter than the approximate period of the oscillators, the stability of the synchronous solution aligns with the stability pattern exhibited by the averaged

network, wherein $H(t) = \begin{bmatrix} d^{-1} & 0 & \dots & 0 \\ 0 & d^{-1} & \ddots & \vdots \\ \vdots & \ddots & \ddots & 0 \\ 0 & \dots & 0 & d^{-1} \end{bmatrix}$. Additionally, it

has been established in Ref. 41 that the stability of such networks, whether they exhibit fast blinking or involve multiple couplings (average network) while maintaining an equivalent synchronization cost (the sum of coupling values), adheres to a linear stability pattern with a slope of $-\frac{1}{d}$ (for a d -dimensional system). In mathematical terms, this pattern can be expressed as $\Lambda = \Lambda_0 - \frac{\kappa}{d}$, where Λ_0 represents the largest Lyapunov exponent of an isolated system. Hence, depending on the value of Λ_0 , it is conceivable that networks with fast-blinking dynamics may undergo an improvement in synchronization.

In the context of the proposed adaptive blinking network, where the coupling scheme $H(t)$ lacks a predefined pattern and remains unpredictable without numerical solutions, the MSF technique proves impractical for delivering analytical stability assessments of the network's synchronization state. Consequently, we resort to numerical methods and employ the synchronization error

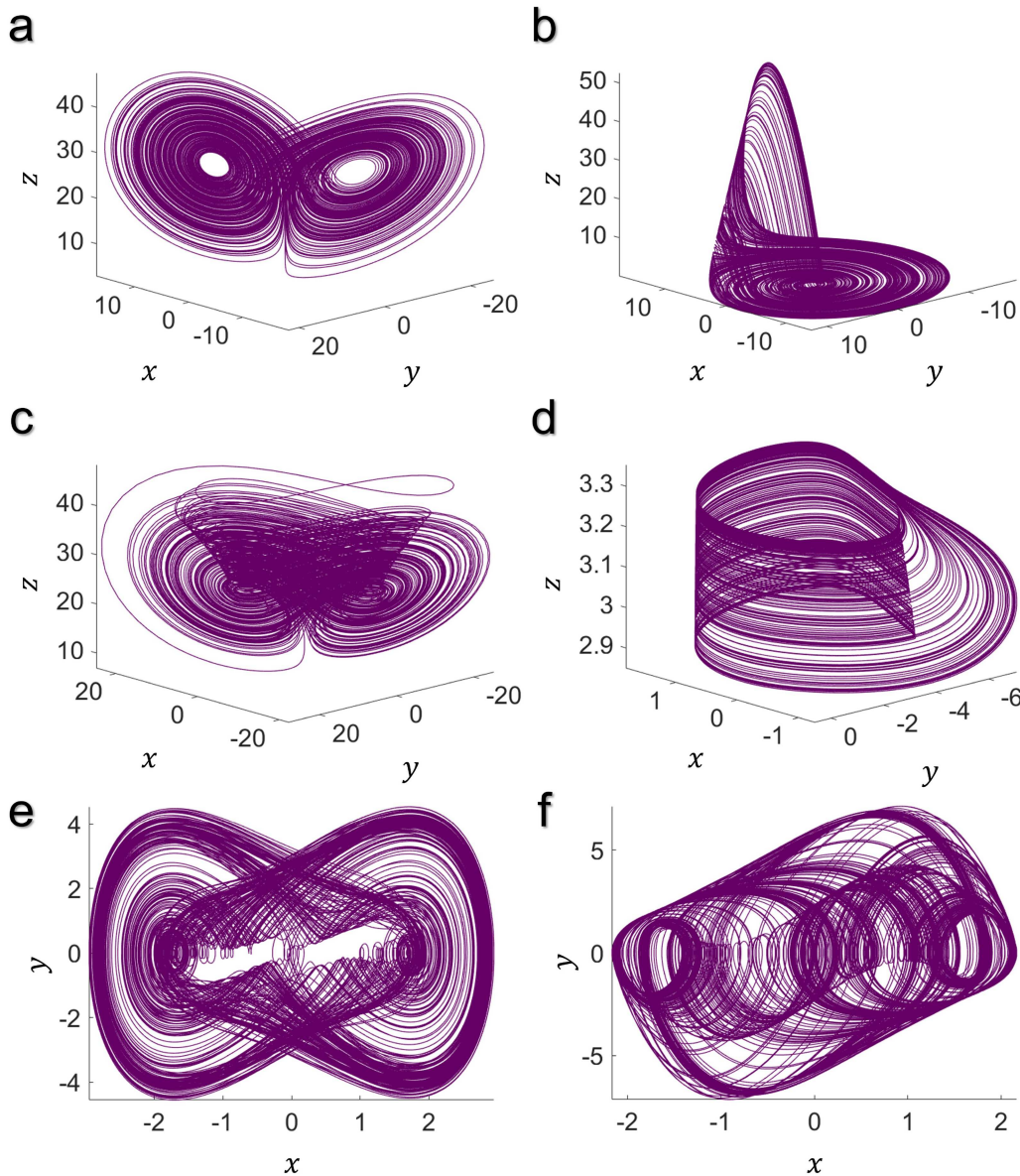


FIG. 1. The phase portraits of the chaotic solutions for (a) the Lorenz system with $(\sigma, \rho, \beta) = (10, 28, 2)$, (b) the Rössler system with $(\alpha, \beta, \gamma) = (0.2, 0.2, 9)$, (c) the Chen system with $(a, c, \beta) = (35, 28, 8/3)$, (d) the HR system with $(l, r, s) = (3.2, 0.006, 4)$, (e) the forced Duffing system with $(\eta, h, q) = (1, 0.1, 5.6)$, and (f) the forced van der Pol system with $(d, F, \eta) = (3, 15, 4.065)$. The initial conditions are considered $(x_0, y_0, z_0) = (1, 1, 1)$ to achieve the Lorenz and Chen attractors, $(x_0, y_0, z_0) = (0, 0, 0)$ to achieve the Rössler and forced Duffing attractors, and $(x_0, y_0, z_0) = (0.1, 0, 0)$ to achieve the HR and forced van der Pol attractors. The system parameters remained consistent with those specified in Ref. 43

as a means to evaluate the network’s synchronizability. The synchronization error, denoted as E_{sync} , can be calculated using the following equation:

$$E_{sync} = \frac{1}{N-1} \left\langle \sum_{j=2}^N \|X_j(t) - X_1(t)\| \right\rangle_T. \quad (5)$$

Here, the symbol $\langle \cdot \rangle$ represents the averaging process throughout run time denoted as T after transient dynamics have been eliminated. In the subsequent section, through simulations conducted on various well-known systems, we demonstrate that implementing adaptive blinking can improve the synchronization state of these systems compared to networks with constant and traditional blinking schemes.

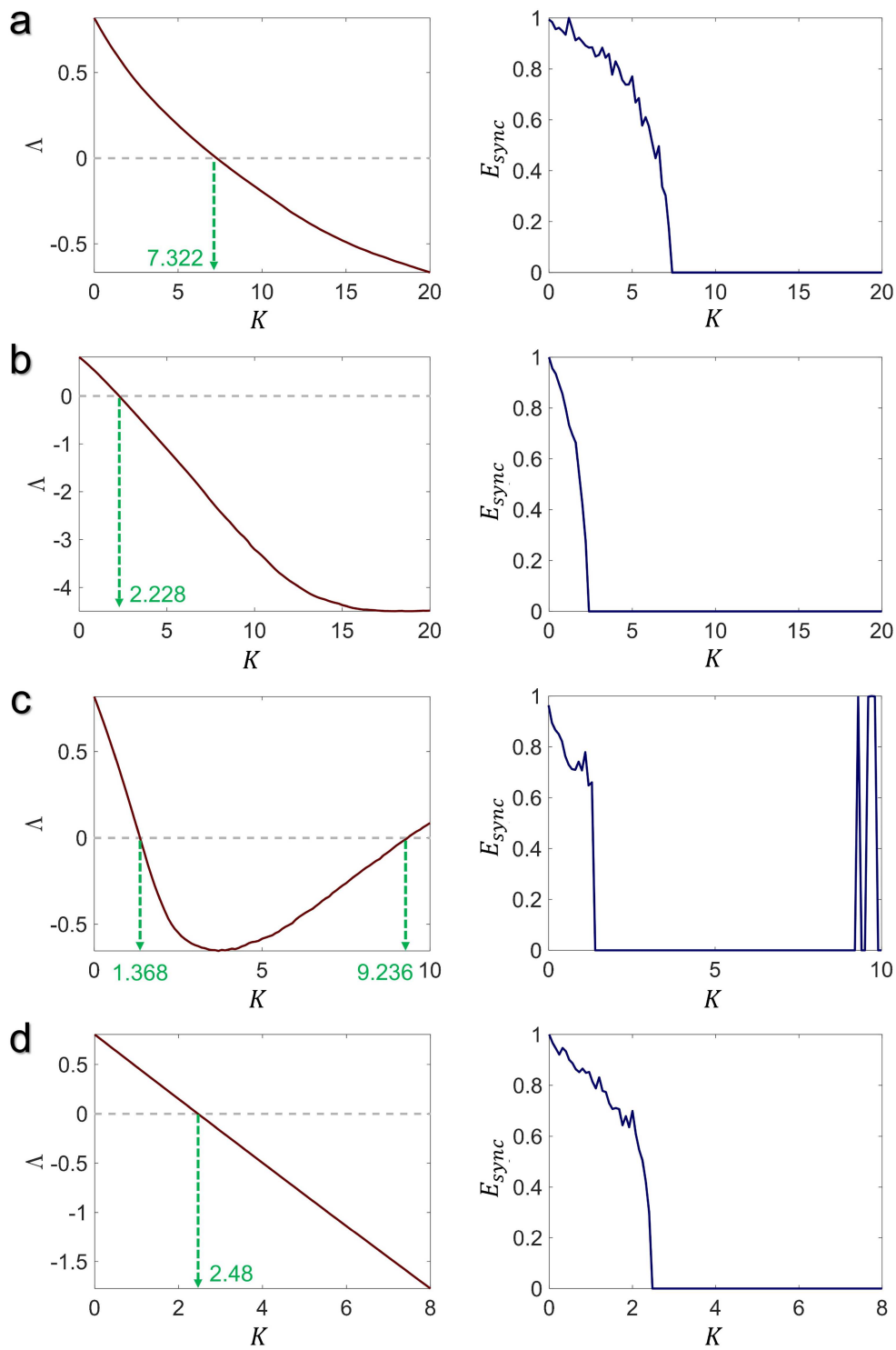


FIG. 2. The MSF (left panel) and the synchronization error (right panel) of two coupled Lorenz systems in (a) $1 \rightarrow 1$ (for $0 \leq K \leq 20$), (b) $2 \rightarrow 2f$ (for $0 \leq K \leq 20$), (c) $3 \rightarrow 3$ (for $0 \leq K \leq 10$), and (d) fast-blinking (for $0 \leq K \leq 8$, and $\tau = 0.03$) coupling schemes. The system parameters are the same as those in Fig. 1(a), and initial conditions are randomly distributed around $(x_0, y_0, z_0) = (1, 1, 1)$. The zero-crossing point(s) of K , at which $\Delta < 0$, are indicated with the green dashed line.

02 August 2024 08:45:09

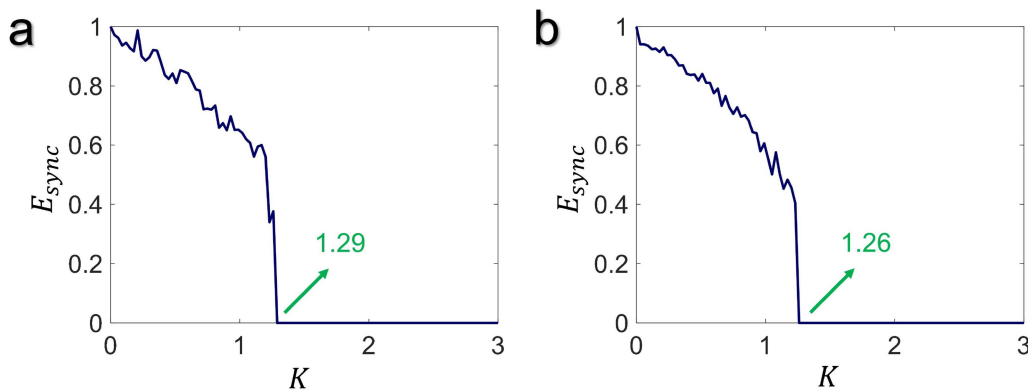


FIG. 3. The synchronization error of the adaptive blinking Lorenz network for $0 \leq K \leq 3$ with $N = 2$, (a) before and (b) after the normalization process. The system parameter settings are the same as in Fig. 1(a), and the initial conditions are randomly selected closely around $(x_0, y_0, z_0) = (1, 1, 1)$. The value of the coupling parameter K at which $E_{sync} = 0$ is marked with the solid arrow.

III. RESULTS

In this section, our analysis encompasses the calculation of MSFs and synchronization errors for both conventional networks characterized by time-constant couplings (specifically, the $1 \rightarrow 1$, $2 \rightarrow 2$, and $3 \rightarrow 3$ configurations) and time-varying networks by fast-blinking coupling functions. Subsequently, we proceed to compute the synchronization error for networks implementing an adaptive blinking coupling scheme, both with and without the normalization process, as detailed in Eqs. (2) and (3). In each scenario, we pinpoint the precise value of the coupling parameter K at which Λ turns negative and E_{sync} reaches zero. This approach enables us to assess the impact of the adaptive blinking framework on network synchronization across varying conditions and configurations. For network construction, six renowned chaotic systems are incorporated, namely, the Lorenz [Fig. 1(a)], Rössler [Fig. 1(b)], Chen [Fig. 1(c)], Hindmarsh–Rose [HR; Fig. 1(d)], forced Duffing [Fig. 1(e)], and forced van der Pol [Fig. 1(f)] systems. In the numerical analysis, the fourth-order Runge–Kutta method with a time step of 0.005 and a run time of 10 000 time units is utilized to compute the synchronization errors and employed Lyapunov analysis to derive the MSFs. This methodology allows for a comprehensive assessment of network synchronization across these diverse chaotic systems. It is important to note that in the calculation of the synchronization error, a network comprising $N = 2$ coupled oscillators with $L = \begin{bmatrix} 1 & -1 \\ -1 & 1 \end{bmatrix}$ is taken into consideration. The method’s versatility is also verified through simulating a larger network of HR systems.

A. Lorenz system

Letting $F(X_i)$ describe the dynamics of the Lorenz system, which can be defined as follows:⁴⁵

$$F(X_i) = \begin{cases} \dot{x}_i = \sigma(y_i - x_i), \\ \dot{y}_i = x_i(\rho - z_i) - y_i, \\ \dot{z}_i = x_i y_i - \beta z_i, \end{cases} \quad (6)$$

where x , y , and z are the state variables, and σ , ρ , and β are the system control parameters. When the system is defined with the parameters $\sigma = 10$, $\rho = 28$, and $\beta = 2$ and initialized with $(x_0, y_0, z_0) = (1, 1, 1)$, as depicted in Fig. 1(a), the chaotic nature of the Lorenz attractor can be observed. The stability of the synchronization state in coupled Lorenz systems is illustrated in Fig. 2, where both MSF and synchronization error metrics are employed to assess synchronization performance under various coupling configurations. Figures 2(a)–2(c) pertain to scenarios with time-constant coupling functions, denoted as the $1 \rightarrow 1$ (for $0 \leq K \leq 20$), $2 \rightarrow 2$ (for $0 \leq K \leq 20$), and $3 \rightarrow 3$ (for $0 \leq K \leq 10$) schemes, respectively, while Fig. 2(d) corresponds to the fast-blinking network with a blinking period of $\tau = 0.03$ and $0 \leq K \leq 8$. Within the examined range of the parameter K , as illustrated in Fig. 2, synchronization in the Lorenz network is attainable for different conditions:

- For constant coupling schemes (the three cases: $1 \rightarrow 1$, $2 \rightarrow 2$, and $3 \rightarrow 3$), synchronization is achieved for $K \geq 7.322$, $K \geq 2.228$, and $1.368 \leq K \leq 9.236$, respectively.
- For the fast-blinking network with coupling changing at each period τ over the total time T , synchronization is achieved for $K \geq 2.48$.

Notably, among these scenarios, the $3 \rightarrow 3$ coupling design results in the lowest synchronization cost. Here, fast-blinking coupling does not contribute to enhancing synchronization. Nonetheless, Fig. 3(a) illustrates the synchronization error of the network with adaptive blinking before normalization, and Fig. 3(b) shows the synchronization error after the normalization process for $0 \leq K \leq 3$. It becomes evident that adaptive blinking coupling enhances synchronization, as the network achieves synchrony for $K \geq 1.29$ without normalization and for $K \geq 1.26$ with the normalization factor applied.

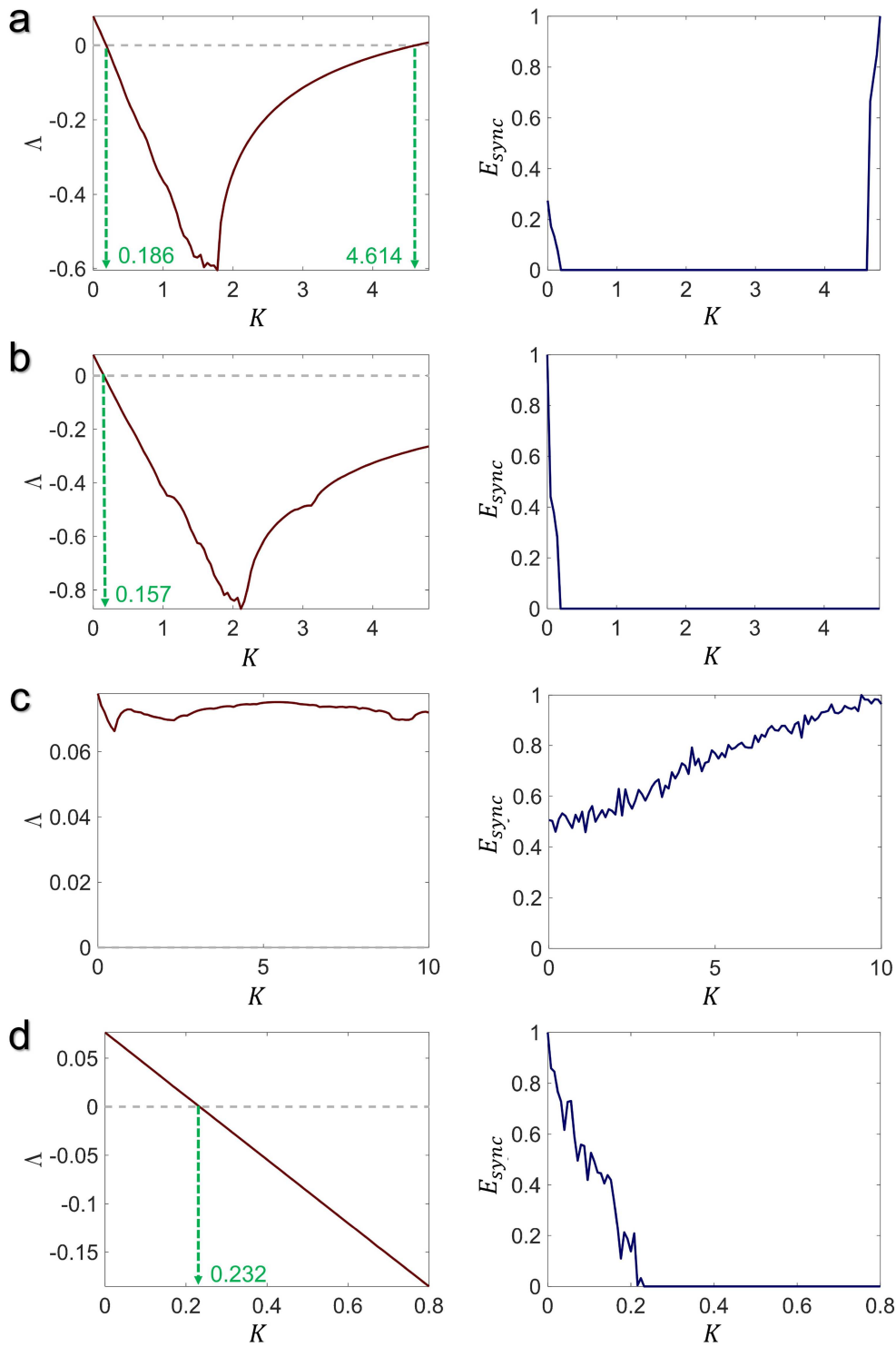


FIG. 4. The MSF (left panel) and the synchronization error (right panel) of two coupled Rössler systems in (a) $1 \rightarrow 1$ (for $0 \leq K \leq 4.8$), (b) $2 \rightarrow 2$ (for $0 \leq K \leq 4.8$), (c) $3 \rightarrow 3$ (for $0 \leq K \leq 10$), and (d) fast-blinking (for $0 \leq K \leq 0.8$, and $\tau = 0.03$) coupling schemes. The system parameters are the same as those in Fig. 1(b), and initial conditions are randomly distributed around $(x_0, y_0, z_0) = (0, 0, 0)$. The zero-crossing point(s) of K , at which $\Delta < 0$, are indicated with the green dashed line.

02 August 2024 08:45:09

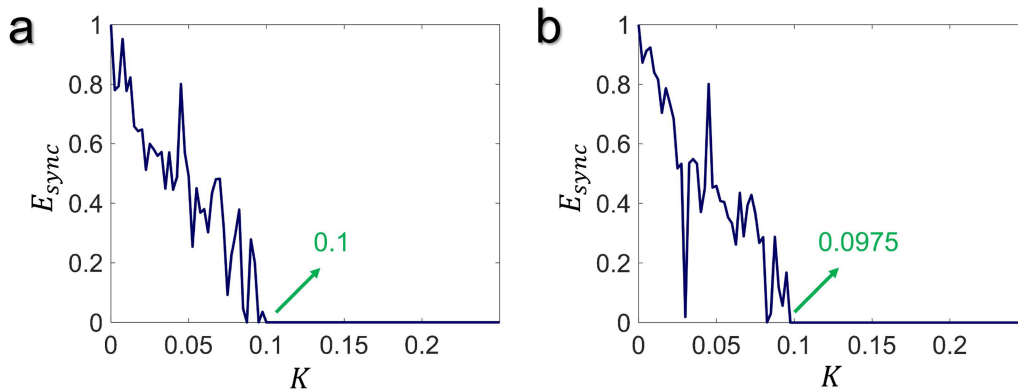


FIG. 5. The synchronization error of the adaptive blinking Rössler network for $0 \leq K \leq 0.25$ with $N = 2$, (a) before and (b) after the normalization process. The system parameter settings are the same as in Fig. 1(b), and the initial conditions are randomly selected closely around $(x_0, y_0, z_0) = (0, 0, 0)$. The value of the coupling parameter K at which $E_{sync} = 0$ is marked with the solid arrow.

B. Rössler system

Taking the Rössler system as the node’s dynamics, $F(X_i)$ is expressed as the follows:⁴⁶

$$F(X_i) = \begin{cases} \dot{x}_i = -y_i - z_i, \\ \dot{y}_i = x_i + \alpha y_i, \\ \dot{z}_i = \beta + (x_i - \gamma)z_i, \end{cases} \quad (7)$$

where $x, y,$ and z are the system variables, and $\alpha, \beta,$ and γ are the system parameters under which the system exhibits different periodic and chaotic behaviors. As demonstrated in Fig. 1(b), the Rössler system exhibits chaotic behavior for $\alpha = 0.2, \beta = 0.2,$ and $\gamma = 9$ assuming the initial condition of $(x_0, y_0, z_0) = (0, 0, 0)$. In Fig. 4, the left panels display the MSFs, while the right panels depict synchronization errors for the Rössler system when organized within a network. The network configurations considered are $1 \rightarrow 1, 2 \rightarrow 2, 3 \rightarrow 3,$ and fast blinking (with $\tau = 0.03$) coupling functions, each over $0 \leq K \leq 4.8, 0 \leq K \leq 4.8, 0 \leq K \leq 10,$ and $0 \leq K \leq 0.8,$ respectively. Within the specified intervals of $K,$ synchronization is attained in different coupling schemes for the Rössler system,

- For the $1 \rightarrow 1$ coupling scheme, synchronization occurs in $0.186 \leq K \leq 4.614.$
- In the $2 \rightarrow 2$ coupling scheme, synchronization is achieved for $K \geq 0.157.$
- In the fast blinking with $\tau = 0.03,$ synchronization occurs for $K \geq 0.232.$

Notably, the $3 \rightarrow 3$ coupling scheme appears to not result in complete synchronization as no value of K is found within the explored parameter range where $\Lambda < 0$ and $E_{sync} = 0.$ This signifies that full synchronization remains elusive under this particular coupling configuration for the Rössler system. The fast blinking coupling scheme does not enhance synchronization for the Rössler system since the synchronization is achieved at a lower value of K when employing the $2 \rightarrow 2$ configuration. Therefore, $2 \rightarrow 2$ coupling outperforms the fast-blinking scheme in terms of achieving the synchronization state. The results of adaptive blinkings on the

network synchronization are demonstrated in Fig. 5. It is noticeable that when the coupling is adaptively selected, synchronization can be achieved for $K \geq 0.1.$ In addition, after applying the normalization process, this threshold decreases even further to $K \geq 0.0975,$ indicating a significant enhancement in synchronization.

C. Chen’s system

Assuming $F(X_i)$ pursues the dynamics of Chen’s system as the nodal dynamics of the network, we have⁴⁷

$$F(X_i) = \begin{cases} \dot{x}_i = a(y_i - x_i), \\ \dot{y}_i = (c - a - z_i)x_i + cy_i, \\ \dot{z}_i = x_i y_i - \beta z_i, \end{cases} \quad (8)$$

where $x, y,$ and z are the states of Chen’s system, and the parameters are $a, c,$ and $\beta.$ By configuring Chen’s system with the parameters $a = 35, c = 28,$ and $\beta = 8/3$ and initializing it with $(x_0, y_0, z_0) = (1, 1, 1),$ Fig. 1(c) illustrates the chaotic dynamics exhibited by Chen’s system under these specified conditions. Figure 6 provides an overview of the synchronization stability analysis results for Chen’s network. The left panels illustrate the MSFs, while the right panels depict synchronization errors. These analyses are conducted for various coupling schemes, namely, $1 \rightarrow 1, 2 \rightarrow 2,$ and $3 \rightarrow 3$ designs, with parameter exploration in the following ranges: $0 \leq K \leq 10, 0 \leq K \leq 10,$ and $0 \leq K \leq 25,$ respectively. Additionally, a time-varying coupling scheme under fast blinking, with a period of $\tau = 0.03,$ is examined within the parameter range of $0 \leq K \leq 20.$ As discerned from the analysis presented in Fig. 6, it becomes evident that the network fails to achieve synchronization when employing $1 \rightarrow 1$ coupling. However, synchronization is observed within specific parameter ranges for other coupling schemes as follows:

- For the $2 \rightarrow 2$ coupling scheme, synchronization is achieved for $K \geq 3.541.$
- In the case of the $3 \rightarrow 3$ coupling scheme, synchronization occurs within $5.347 \leq K \leq 21.51.$

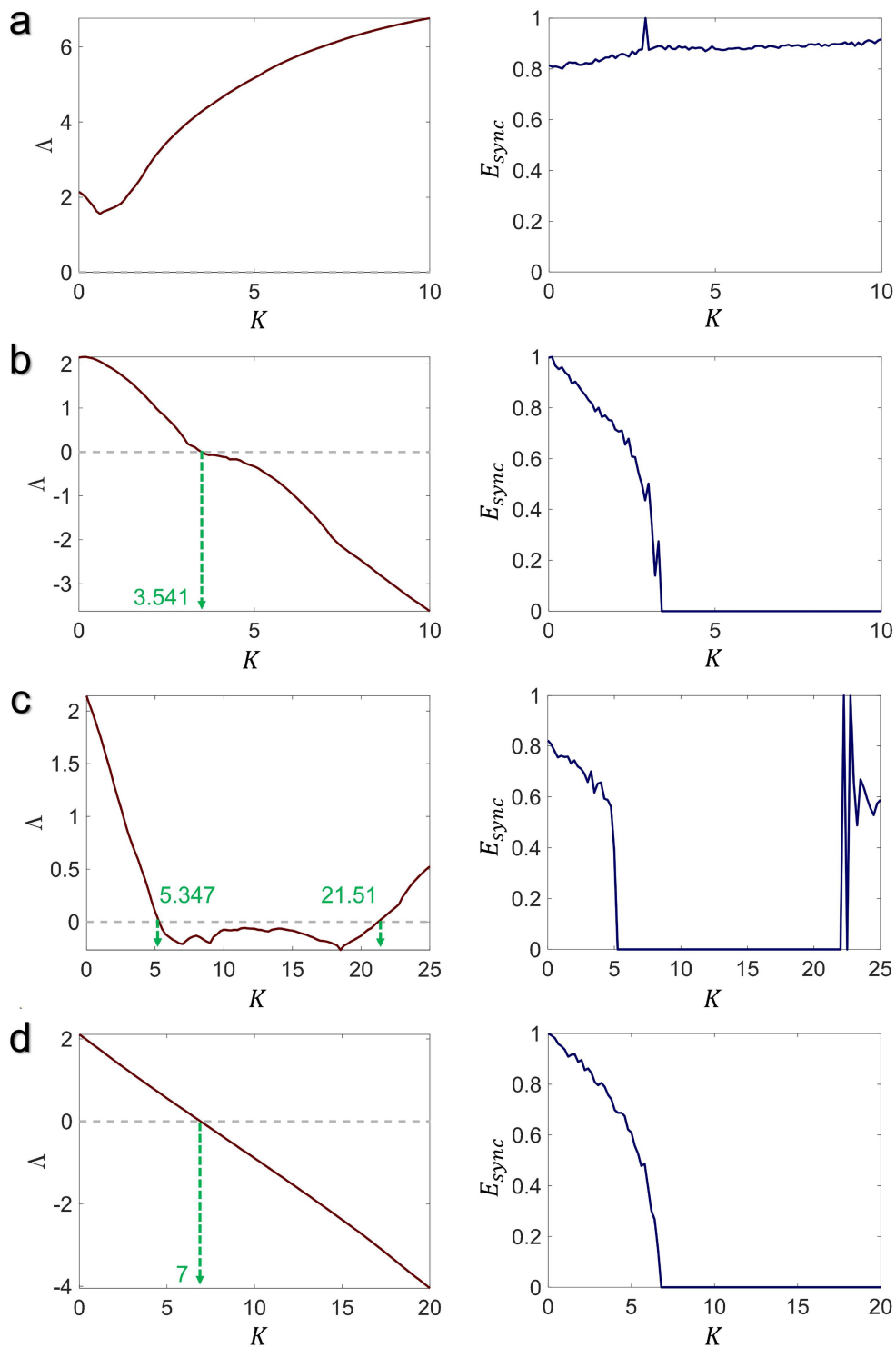


FIG. 6. The MSF (left panel) and the synchronization error (right panel) of two coupled Chen's systems in (a) $1 \rightarrow 1$ (for $0 \leq K \leq 10$), (b) $2 \rightarrow 2$ (for $0 \leq K \leq 10$), (c) $3 \rightarrow 3$ (for $0 \leq K \leq 25$), and (d) fast blinking (for $0 \leq K \leq 20$, and $\tau = 0.03$) coupling schemes. The system parameters are the same as those in Fig. 1(c), and initial conditions are randomly distributed around $(x_0, y_0, z_0) = (1, 1, 1)$. The zero-crossing point(s) of K , at which $\Delta < 0$, are indicated with the green dashed line.

02 August 2024 08:45:09

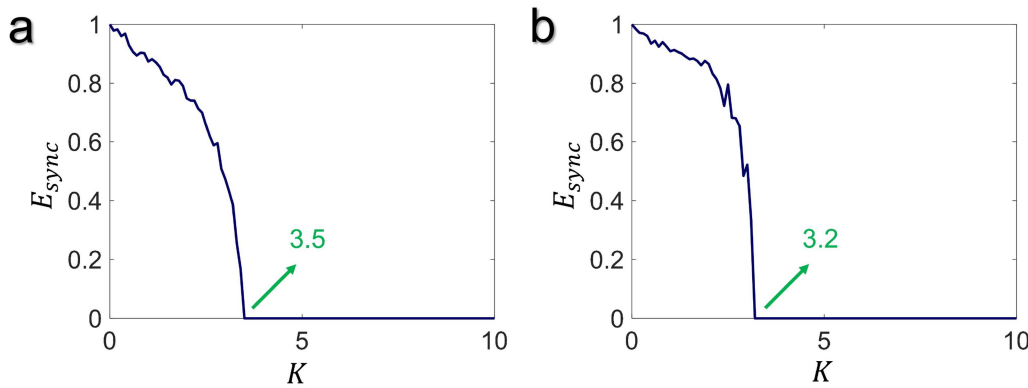


FIG. 7. The synchronization error of the adaptive blinking Chen’s network for $0 \leq K \leq 10$ with $N = 2$, (a) before and (b) after the normalization process. The system parameter settings are the same as in Fig. 1(c), and the initial conditions are randomly selected closely around $(x_0, y_0, z_0) = (1, 1, 1)$. The value of the coupling parameter K at which $E_{sync} = 0$ is marked with the solid arrow,

- Under the fast-blinking scheme, synchronization is attained for $K \geq 7$.

Note that for time-constant couplings, the reported synchronization regions are valid for the studied range of parameter K . It is observed that the network achieves synchronization with the lowest K value under the $2 \rightarrow 2$ coupling rather than the fast-blinking scheme. The synchronization assessment of the network employing adaptive blinking coupling is presented in Fig. 7 through synchronization error. Notably, the adaptive switching between couplings results in synchronization at lower K values as $K \geq 3.5$ before and $K \geq 3.2$ after involving the normalization factor.

D. HR system

Considering $F(X_i)$ follows the dynamics of the HR system according to the following set of equations:⁴⁸

$$F(X_i) = \begin{cases} \dot{x}_i = y_i + 3x_i^2 - x_i^3 - z_i + I, \\ \dot{y}_i = 1 - 5x_i^2 - y_i, \\ \dot{z}_i = -rz_i + rs(x_i + 1.6), \end{cases} \quad (9)$$

where the state variables of the system are denoted by $x, y,$ and $z,$ and the system’s parameters are $I, r,$ and $s.$ According to Fig. 1(d), for $I = 3.2, r = 0.006,$ and $s = 4,$ the HR system exhibits a chaotic dynamics initialized by $(x_0, y_0, z_0) = (0.1, 0, 0).$ The MSF (left panels) and the synchronization error (right panels) diagrams featured in Fig. 8 provide insights into the synchronization stability analysis of the HR network. The analyses are conducted for different coupling configurations, i.e., $1 \rightarrow 1, 2 \rightarrow 2, 3 \rightarrow 3,$ and fast blinking (with $\tau = 0.03$), with parameter exploration in the following ranges: $0 \leq K \leq 5, 0 \leq K \leq 5, 0 \leq K \leq 10, 0 \leq K \leq 0.15,$ respectively. In the HR network, it is noteworthy that synchronization to a common temporal pattern is observed within specific parameter ranges for various coupling schemes, except for the $3 \rightarrow 3$ scheme. Here are the synchronization regions for the HR network within the determined range of the parameter $K:$

- For constant coupling schemes (the two cases: $1 \rightarrow 1$ and $2 \rightarrow 2$), synchronization is achieved for $K \geq 0.94$ and $K \geq 0.094,$ respectively.
- For the fast-blinking network with coupling changing at each period τ over the total time $T,$ synchronization is achieved for $K \geq 0.0405.$

Here, it is apparent that the fast-blinking coupling scheme proves to be effective in enhancing synchronization within the HR network since the synchronization incident is observed for the lowest value of K compared to other cases, underscoring the advantage of fast-blinking coupling in promoting synchronization in the HR network. The synchronization error analysis of the HR network employing adaptive blinking, both with and without the normalization consideration, is depicted in Fig. 9. Notably, without the normalization process, no significant improvement in synchronization is observed ($K \geq 0.46$), compared to the fast-blinking network. However, after the normalization, synchronization experiences a substantial enhancement ($K \geq 0.033$).

E. Forced Duffing system

Let us contemplate the utilization of the forced Duffing system to characterize the behavior of the nodes within the network, as expressed by the following equations:⁴⁹

$$F(X_i) = \begin{cases} \dot{x}_i = y_i, \\ \dot{y}_i = -hy_i - x_i^3 + q \sin(\eta t), \end{cases} \quad (10)$$

which can be rewritten in an autonomous form as follows:

$$F(X_i) = \begin{cases} \dot{x}_i = y_i, \\ \dot{y}_i = -hy_i - x_i^3 + q \sin(\eta z_i), \\ \dot{z}_i = 1, \end{cases} \quad (11)$$

with x, y, z as state variables and $h, q,$ and η as the system parameters. The chaotic attractor of the forced Duffing system, characterized by parameters $h = 0.1, q = 5.6,$ and $\eta = 1$ and the initial condition

02 August 2024 08:45:09

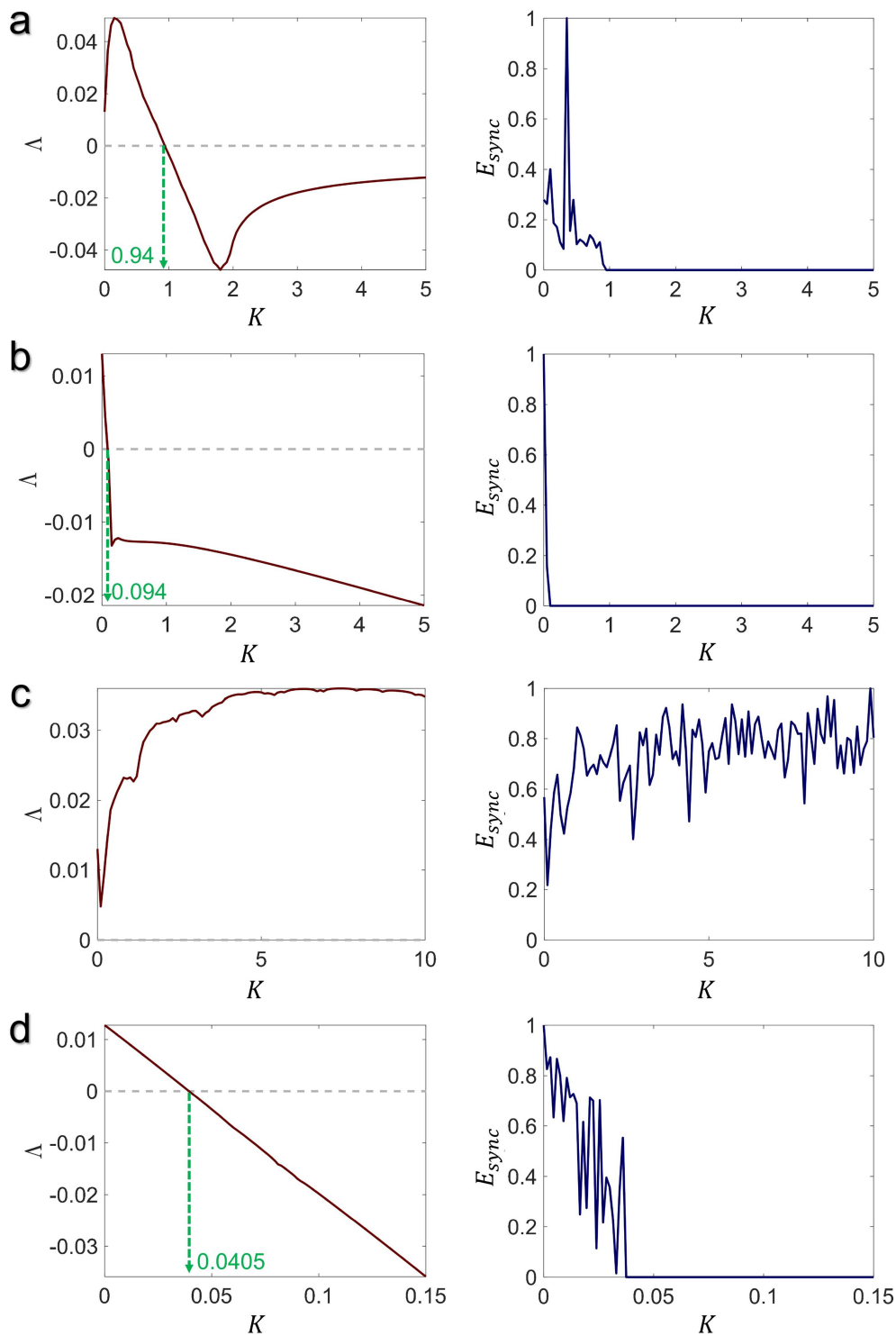


FIG. 8. The MSF (left panel) and the synchronization error (right panel) of two coupled HR systems in (a) $1 \rightarrow 1$ (for $0 \leq K \leq 5$), (b) $2 \rightarrow 2f$ (or $0 \leq K \leq 5$), (c) $3 \rightarrow 3$ (for $0 \leq K \leq 10$), and (d) fast-blinking (for $0 \leq K \leq 0.15$, and $\tau = 0.03$) coupling schemes. The system parameters mirror those in Fig. 1(d), and initial conditions are randomly distributed around $(x_0, y_0, z_0) = (0.1, 0, 0)$. The zero-crossing point(s) of K , at which $\Delta < 0$, are indicated with the green dashed line.

02 August 2024 08:45:09

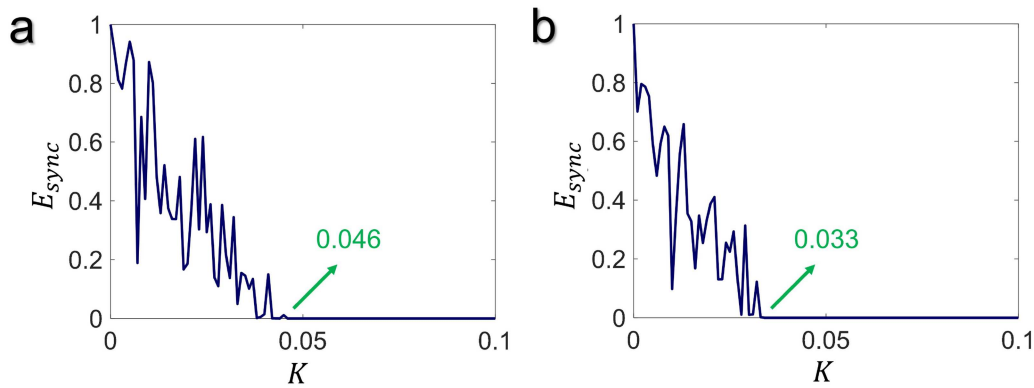


FIG. 9. The synchronization error of the adaptive blinking HR network for $0 \leq K \leq 0.1$ with $N = 2$, (a) before and (b) after the normalization process. The system parameter settings are the same as in Fig. 1(d), and the initial conditions are randomly selected closely around $(x_0, y_0, z_0) = (0.1, 0, 0)$. The value of the coupling parameter K at which $E_{sync} = 0$ is marked with the solid arrow.

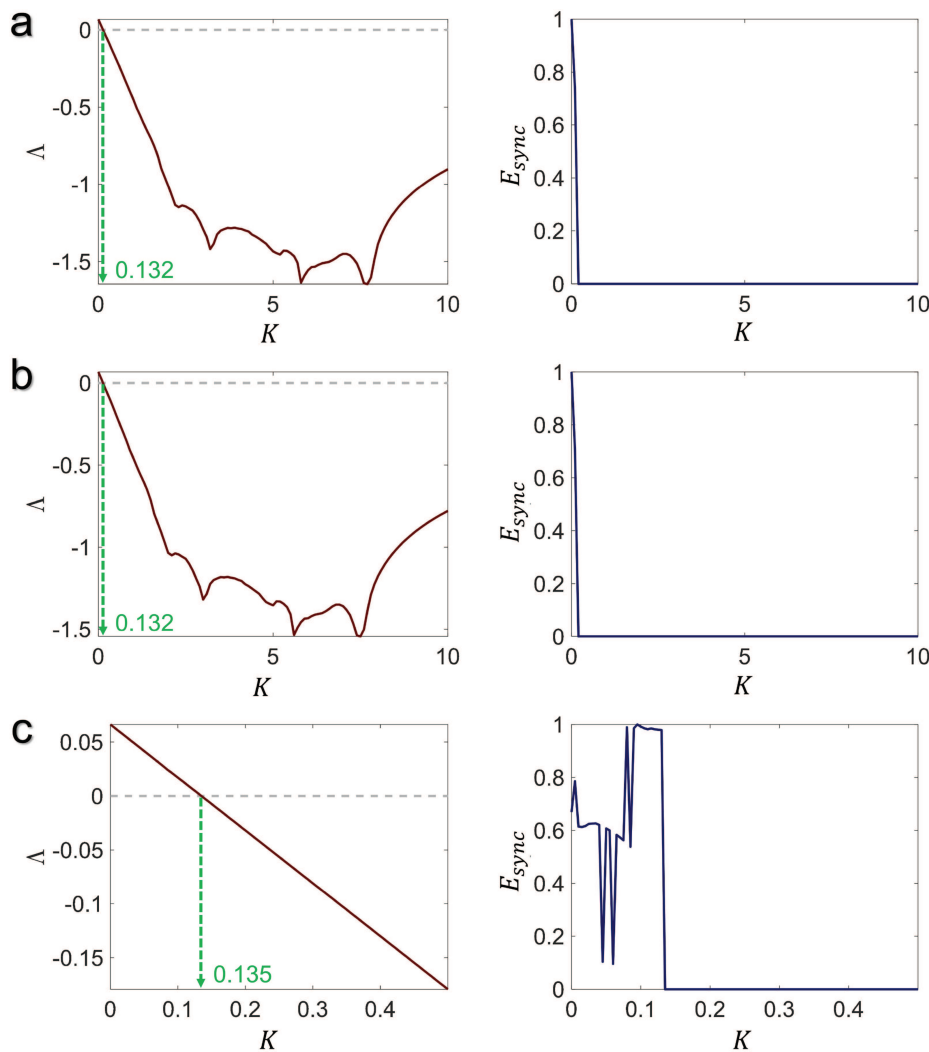


FIG. 10. The MSF (left panel) and the synchronization error (right panel) of two coupled forced Duffing systems in (a) $1 \rightarrow 1$ (for $0 \leq K \leq 10$), (b) $2 \rightarrow 2$ (for $0 \leq K \leq 10$), and (c) fast-blinking (for $0 \leq K \leq 0.5$, and $\tau = 0.02$) coupling schemes. The system parameters are the same as those in Fig. 1(e), and initial conditions are randomly distributed around $(x_0, y_0, z_0) = (0, 0, 0)$. The zero-crossing point(s) of K , at which $\Delta < 0$, are indicated with the green dashed line.

02 August 2024 08:45:09

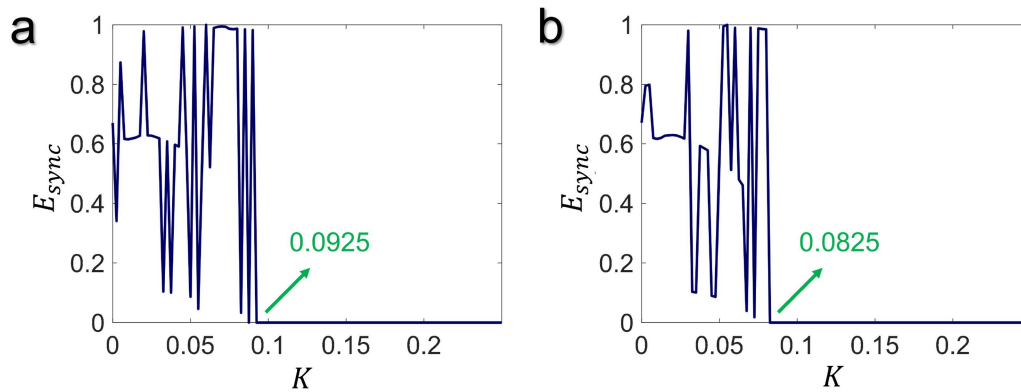


FIG. 11. The synchronization error of the adaptive blinking forced Duffing network for $0 \leq K \leq 0.25$ with $N = 2$, (a) before and (b) after the normalization process. The system parameter settings are the same as in Fig. 1(e), and the initial conditions are randomly selected closely around $(x_0, y_0, z_0) = (0, 0, 0)$. The value of the coupling parameter K at which $E_{sync} = 0$ is marked with the solid arrow.

$(x_0, y_0, z_0) = (0, 0, 0)$, is presented in Fig. 1(e). For the stability analysis of the synchronous solution in the forced Duffing network, the MSFs and synchronization errors are illustrated in Fig. 10. These results are organized into left and right panels and correspond to various coupling configurations, including $1 \rightarrow 1$ (for $0 \leq K \leq 10$), $2 \rightarrow 2$ (for $0 \leq K \leq 10$), and the fast-blinking (for $0 \leq K \leq 0.5$ and $\tau = 0.02$) schemes. In the self-contained description of the forced Duffing oscillator, as presented in Eq. (11), the inclusion of the variable z serves to mimic the influence of time t on the system. Hence, within blinking-based coupling configurations, the $3 \rightarrow 3$ scheme is excluded from consideration in the analysis of synchronization. The analysis presented in Fig. 10 reveals that within the explored coupling parameter range, synchronization in the forced Duffing network is achieved as follows:

- For time-constant coupling schemes, i.e., the $1 \rightarrow 1$ or $2 \rightarrow 2$ configurations, synchronization occurs for $K \geq 0.132$.
- In the fast-blinking coupling design with the blinking period of $\tau = 0.02$, synchronization is observed for $K \geq 0.135$.

These findings highlight that the fast-blinking coupling configuration does not necessarily lead to enhanced synchronization in the forced Duffing system network. Instead, the smallest K values for achieving synchrony are observed through time-constant coupling configurations, namely, the $1 \rightarrow 1$ or $2 \rightarrow 2$ configurations. Nonetheless, through the synchronization error calculated for $0 \leq K \leq 0.25$, Fig. 11 indicates that network synchronization can be further enhanced when adaptive blinking coupling is involved. More clearly, Fig. 11 shows that via adaptive blinking coupling, the forced Duffing network achieves synchrony for $K \geq 0.0925$, which can be decreased to $K \geq 0.0825$ when the normalization process is involved in the coupling selection process.

F. Froced van der Pol system

As the last studied case, the forced version of the van der Pol system is assumed as the network node dynamics, which obeys the

following equations:⁵⁰

$$F(X_i) = \begin{cases} \dot{x}_i = y_i, \\ \dot{y}_i = -x_i + d(1 - x_i^2)y_i + F \sin(\eta t), \end{cases} \quad (12)$$

where x and y are the state variables and d, F , and η are the system's control parameters. The forced van der Pol system can be represented as an autonomous system by introducing the variable z to emulate the effect of time t . Consequently, in its autonomous form, the forced van der Pol system is defined as follows:

$$F(X_i) = \begin{cases} \dot{x}_i = y_i, \\ \dot{y}_i = -x_i + d(1 - x_i^2)y_i + F \sin(\eta z_i), \\ \dot{z}_i = 1. \end{cases} \quad (13)$$

Figure 1(f) illustrates that when the system parameters are fixed at $d = 3, F = 15$, and $\eta = 4.065$ and initialized with $(x_0, y_0, z_0) = (0.1, 0, 0)$, the forced van der Pol system behaves chaotically. Figure 12 indicates the MSFs in the left panels and synchronization errors in the right panels, in which the stability of the van der Pol network is analyzed for $1 \rightarrow 1$ concerning $0 \leq K \leq 10$, $2 \rightarrow 2$ concerning $0 \leq K \leq 10$, and blinking network with fast switching with $\tau = 0.02$ concerning $0 \leq K \leq 0.6$. As a consequence, within the examined parameter range of K , the network's synchronization behavior is as follows:

- Under the $1 \rightarrow 1$ coupling scheme, synchronization is achieved when $K \geq 0.161$.
- For the $2 \rightarrow 2$ coupling scheme, synchronization emerges for $K \geq 0.316$.
- With the fast-blinking coupling configuration having $\tau = 0.02$, synchronization is attained in $K \geq 0.216$.

It is worth noting that, like the forced Duffing network, the $3 \rightarrow 3$ coupling case is not investigated in this study since the forced van der Pol system is originally a two-dimensional system. Based on the findings presented in Fig. 12, it can be found that when the coupling configuration is set to $1 \rightarrow 1$, the network

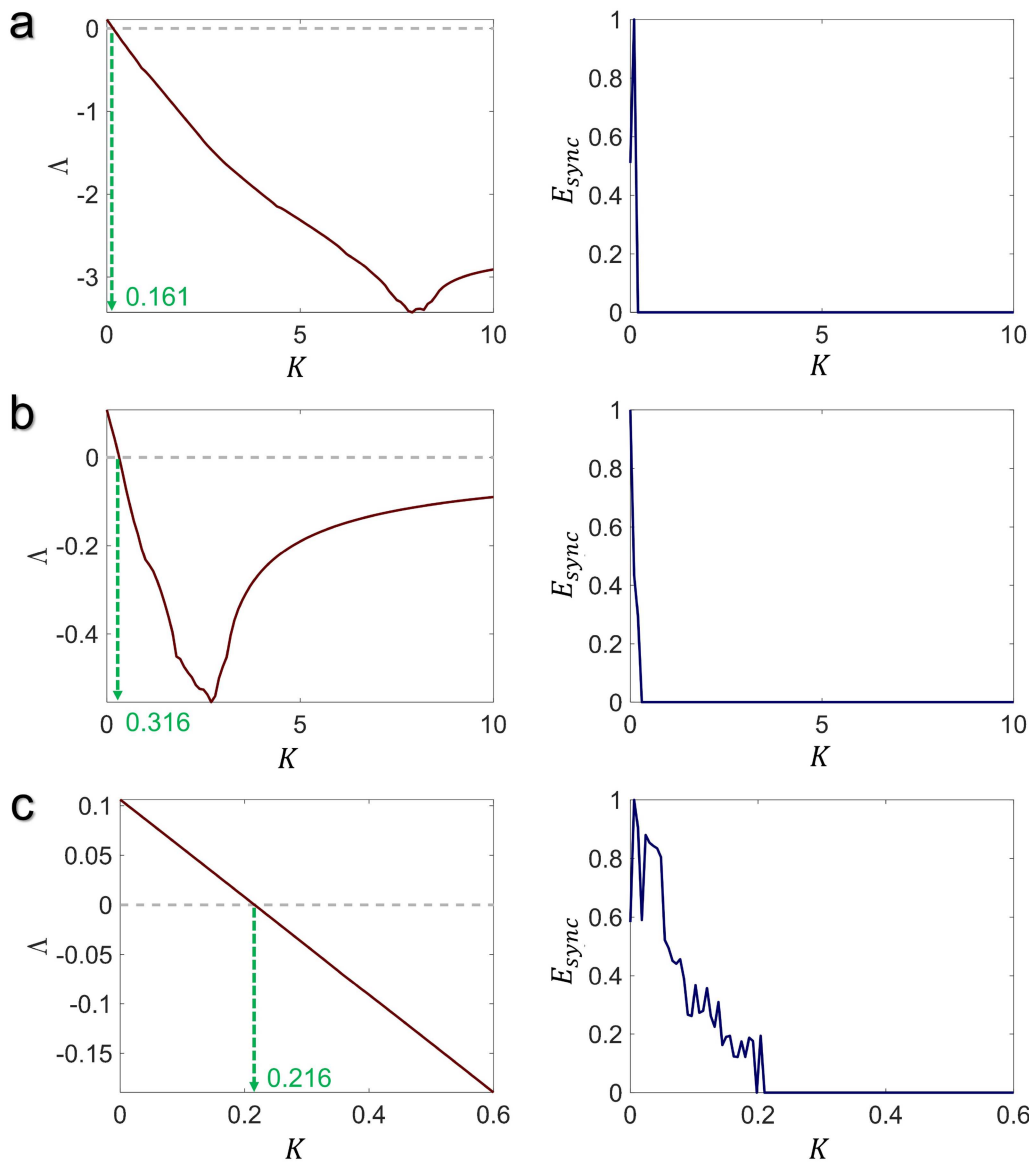


FIG. 12. The MSF (left panel) and the synchronization error (right panel) of two coupled forced van der Pol systems in (a) $1 \rightarrow 1$ (for $0 \leq K \leq 10$), (b) $2 \rightarrow 2$ (for $0 \leq K \leq 10$), and (c) fast-blinking (for $0 \leq K \leq 0.6$, and $\tau = 0.02$) coupling schemes. The system parameters are the same as those in Fig. 1(f), and initial conditions are randomly distributed around $(x_0, y_0, z_0) = (0.1, 0, 0)$. The zero-crossing point(s) of K , at which $\Delta < 0$, are indicated with the green dashed line.

achieves synchronization with the smallest value of parameter K , in comparison with other scenarios, particularly the fast-blinking coupling. In contrast, Fig. 13 refers to the synchronization analysis of the forced van der Pol network with adaptive blinking coupling for $0 \leq K \leq 0.5$. It can be noticed that when the selection of coupling is performed without normalization, the network synchrony is not enhanced since the synchronization is attained for $K \geq 0.22$. However, after applying the normalization process decreases the critical coupling and synchronization can be observed

for $K \geq 0.11$, which is noticeably lower than other coupling scenarios.

G. Universality assessment

Previously reported results demonstrated that the presented adaptive scheme yields notable synchronization improvements compared to constant and fast-blinking coupling schemes. In non-adaptive coupling configurations, the MSF can be reached, serving

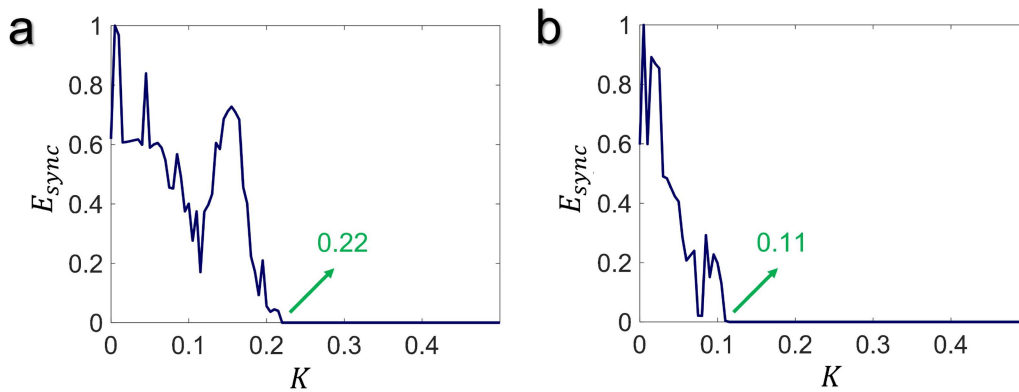


FIG. 13. The synchronization error of the adaptive blinking forced van der Pol network for $0 \leq K \leq 0.5$ with $N = 2$, (a) before and (b) after the normalization process. The system parameter settings are the same as in Fig. 1(f), and the initial conditions are randomly selected closely around $(x_0, y_0, z_0) = (0.1, 0, 0)$. The value of the coupling parameter K at which $E_{sync} = 0$ is marked with the solid arrow.

as a general method to establish synchronization criteria applicable to networks of any size and topology. Consequently, the calculation of the MSF for such coupling schemes serves as evidence of their universality. However, in the proposed adaptive blinking scheme,

achieving the MSF is not feasible due to the inherent indeterministic nature of the couplings. Hence, to ascertain the effectiveness of this method on larger networks or to evaluate its universality, we consider a Watts–Strogatz small-world structure.⁵¹ This

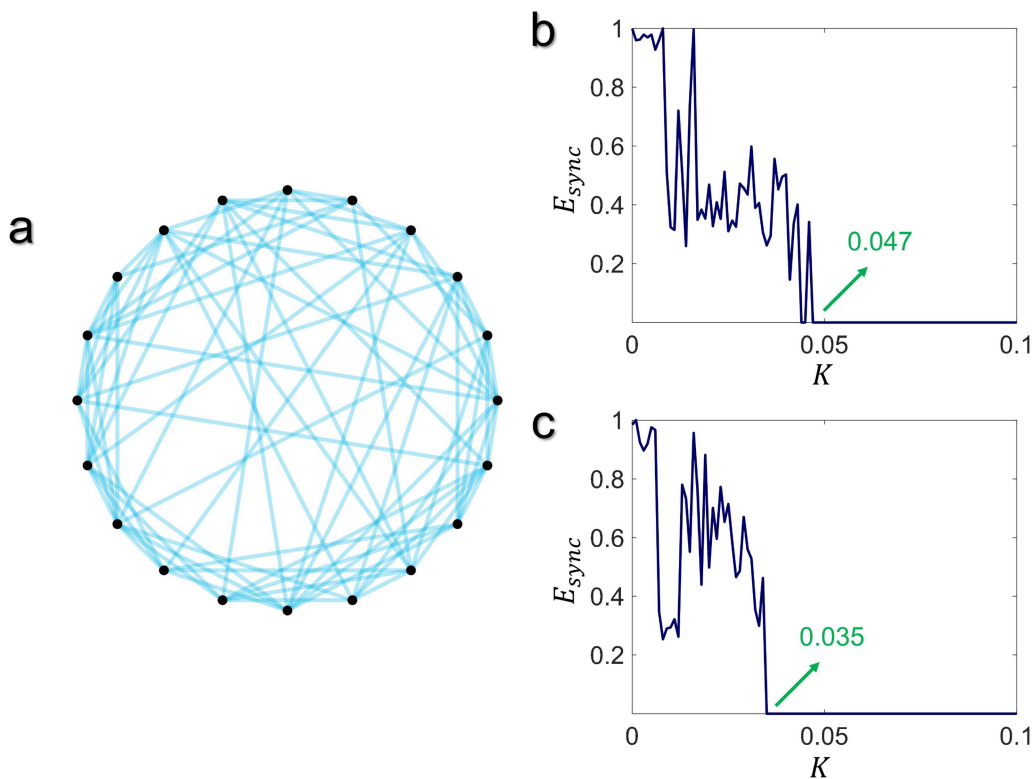


FIG. 14. (a) The graph-based representation of the employed Watts–Strogatz small-world network structure according to,⁵¹ considering $N = 20$ nodes, a mean degree of $d_m = 8$ and a rewiring probability of $p = 0.4$. The synchronization error of the adaptive blinking HR network for $0 \leq K \leq 0.1$ with $N = 20$, (b) before and (c) after the normalization process. The system parameter settings are the same as in Fig. 1(d), and the initial conditions are randomly selected closely around $(x_0, y_0, z_0) = (0.1, 0, 0)$. The value of the coupling parameter K at which $E_{sync} = 0$ is marked with the solid arrow.

02 August 2024 08:45:09

structure comprises $N = 20$ HR systems, with a mean degree of $d_m = 8$ and a rewiring probability of $p = 0.4$, as depicted in Fig. 14(a). Utilizing the definition of the adaptive blinking structure, the synchronization error of the constructed HR network is presented in Figs. 14(b) and 14(c), before and after incorporating the normalization factor as outlined in Eqs. (2) and (3). To have a fair comparison with Fig. 9, the HR systems are set at $I = 3.2$, $r = 0.006$, and $s = 4$. In addition, the initial conditions are randomly selected around $(x_0, y_0, z_0) = (0.1, 0, 0)$.

The results shown in Figs. 14(b) and 14(c) indicate that without the normalization process, the network achieves synchrony for values of $K \geq 0.047$. However, when the normalization factor is introduced into the adaptive blinking process, synchronization is achieved for $K \geq 0.035$, which represents a significant reduction. These synchronization threshold values closely align with those presented in Fig. 9. Therefore, it can be inferred that even for larger networks, here comprising 20 oscillators, the involvement of the normalized adaptive blinking structure can lead to synchronization at lower coupling parameter values compared to other schemes, namely, the constant and fast-blinking coupling structures. In contrast, the unnormalized adaptive blinking scheme does not consistently guarantee an improvement in synchronization.

IV. DISCUSSION AND CONCLUSION

Time-varying networks, particularly those with blinking dynamics, offer a versatile framework for modeling and understanding complex systems. In these networks, connections and interactions evolve dynamically over time, reflecting the temporal nature of many real-world phenomena.⁵² Blinking networks, characterized by intermittent and transient connections, are particularly valuable for studying synchronization, stability, and resilience in various systems.⁵³ They find applications in fields such as neuroscience, where brain regions exhibit dynamic connectivity patterns, and in communication networks, where intermittent link quality is common.^{53,54} Understanding the dynamics of time-varying and blinking networks is essential for uncovering hidden patterns, predicting system behaviors, and designing effective interventions in domains in different fields. Given this significance, certain investigations have concentrated on the variability of either coupling strength^{55–57} or coupling functions.^{42,52,53}

This research explored a novel time-varying coupling function within complex networks. The adaptability of this network arises from the selection of the most efficient coupling scheme at each time step. This selection relies on assessing the differences in the nodal variables. This dynamic coupling setup enables synchronization with a substantially reduced coupling parameter (synchronization cost) compared to when time-constant or periodic blinking coupling is employed. In the process of adaptive selection, it is crucial to accurately evaluate the individual contribution of each variable to synchronization for dependable decisions. Consequently, prior to choosing the coupling scheme, it is essential to normalize the average difference associated with each variable based on the range of solutions within the synchronization state. To illustrate the enhancement in synchronization achieved through presented adaptive coupling, the findings were compared with those obtained from time-constant coupling (i.e., $1 \rightarrow 1$, $2 \rightarrow 2$, and $3 \rightarrow 3$

TABLE I. The summary of findings: Emphasizing the enhancement in synchronization within the adaptive blinking scheme, especially when incorporating normalization factors into the coupling selection procedure, compared to the optimal scenarios of time-constant coupling and periodic blinking schemes.

| Network | Non-adaptive optimal coupling scheme | Adaptive blinking scheme | |
|--------------------|--|--------------------------|---------------------|
| | | Before normalization | After normalization |
| Lorenz | $3 \rightarrow 3$ $1.368 \leq K \leq 9.236$ | $K \geq 1.29$ | $K \geq 1.26$ |
| Rössler | $2 \rightarrow 2$ $K \geq 0.157$ | $K \geq 0.1$ | $K \geq 1.0975$ |
| Chen | $2 \rightarrow 2$ $K \geq 3.541$ | $K \geq 3.5$ | $K \geq 3.2$ |
| HR | Fast blinking $K \geq 0.0405$ | $K \geq 0.046$ | $K \geq 0.033$ |
| Forced Duffing | $1 \rightarrow 1$ or $2 \rightarrow 2$ $K \geq 0.132$ | $K \geq 0.0925$ | $K \geq 0.0825$ |
| Forced van der Pol | $1 \rightarrow 1$ $K \geq 0.161$ | $K \geq 0.22$ | $K \geq 0.11$ |

configurations) and fast-blinking scheme. To this aim, six different networks consisting of identical systems were examined, including Lorenz, Rössler, Chen, HR, forced Duffing, and forced van der Pol systems. The outcomes are briefly presented in Table I. Notably, fast-blinking coupling demonstrates synchronization improvement exclusively for the HR networks, whereas time-constant couplings emerge as the optimal choice in the majority of scenarios. Nonetheless, adaptive blinking coupling without the normalization process leads to enhancement in synchronization except for the HR and forced van der Pol networks. However, incorporating the normalization factors into the selection process shows substantial synchronization improvement across all cases. This outcome underscores the significance of selecting the most dependable coupling scheme at each time step.

An examination of the adaptive blinking scheme within larger networks was conducted to gauge the method's universality. In this regard, a Watts–Strogatz small-world structure containing ten nodes with HR dynamics was considered. The results revealed that synchronization enhancement remains discernible even in larger networks. Note that the outcomes of the larger network were consistent with those observed in two coupled HR systems.

Figure 15 provides insights into the selection of coupling schemes (from the set of all self-couplings in a d -dimensional system) at each instant of the total run time of 10 000 time units. It is noticeable that once the synchronization threshold is surpassed, signified by sufficiently minimal E_{sync} , the network upholds its coupling structure after passing a transient period. The adaptive selection mechanism maintains synchrony even in negligible synchronization deviations ($E_{sync} \approx 0$). Furthermore, the network tends to retain the same structure, which is optimal for synchronization maintenance. Therefore, when a network employing adaptive blinking achieves synchrony, it remains within its synchronous state.

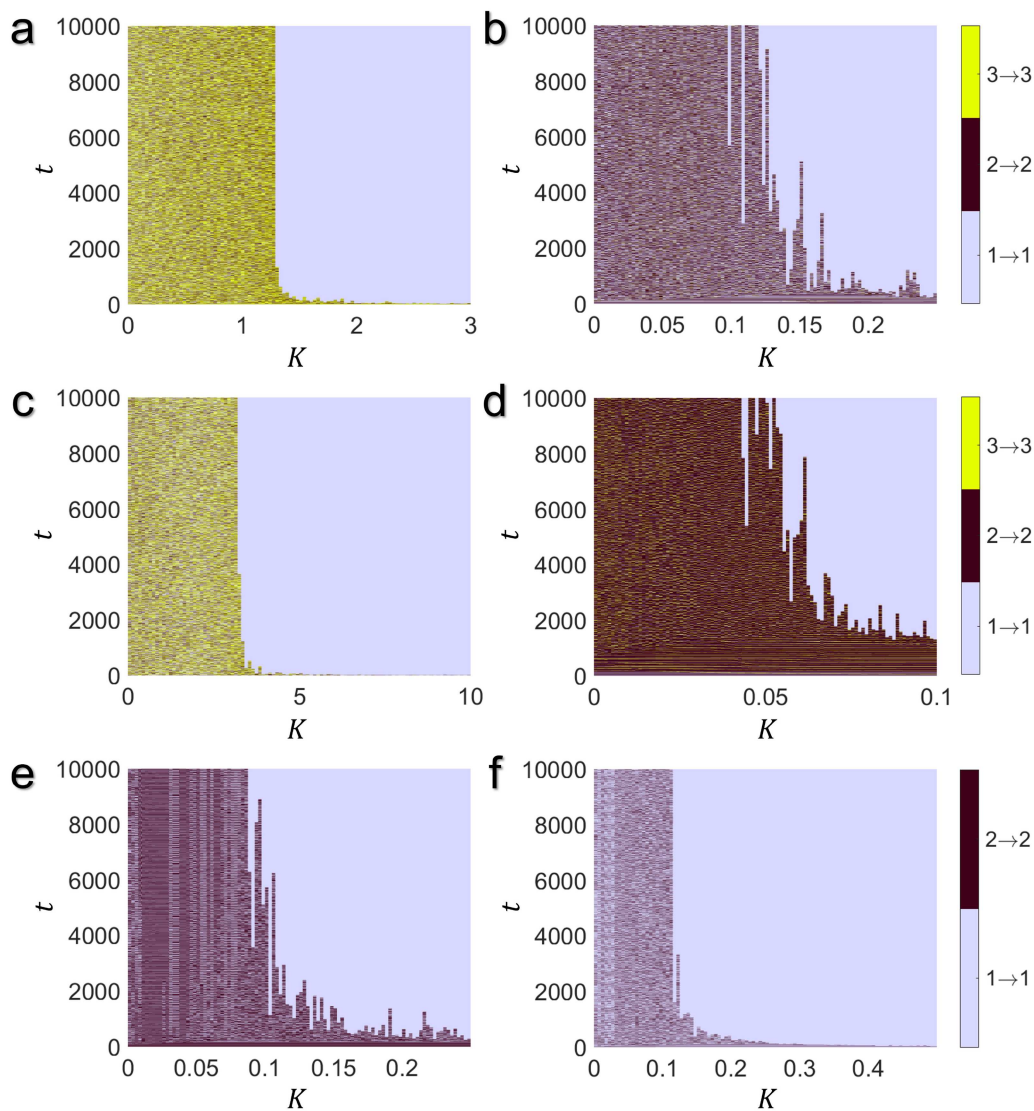


FIG. 15. The coupling selection process involving the normalization factors in the network composed of two coupled (a) Lorenz systems for $0 \leq K \leq 3$ [corresponds to Fig. 3(b)], (b) Rössler systems $0 \leq K \leq 0.25$ [corresponds to Fig. 5(b)], (c) Chen's systems for $0 \leq K \leq 10$ [corresponds to Fig. 7(b)], (d) HR systems for $0 \leq K \leq 0.1$ [corresponds to Fig. 9(b)], (e) forced Duffing systems for $0 \leq K \leq 25$ [corresponds to Fig. 11(b)], and (f) forced van der Pol systems for $0 \leq K \leq 0.5$ [corresponds to Fig. 13(b)], over 10 000 time units. In each time instance t , the selected coupling is coded in light purple for $1 \rightarrow 1$ configuration, dark brown for $2 \rightarrow 2$ configuration, and yellow for $3 \rightarrow 3$ configuration.

The adaptive blinking approach introduced in this study is not confined to diffusive couplings and can be applied in any network design. However, in the case of other coupling schemes, such as memristor couplings, which introduce a new system state^{58,59} or chemical couplings,⁶⁰ it is not anticipated that the introduced adaptation criteria would necessarily result in enhanced synchronization. The reason is that the adaptation scheme is designed based on the nature of diffusive or feedback couplings. Nevertheless, the adaptation scheme can be refined and adjusted in accordance with the

specific coupling scheme, and this remains an objective for future studies. Furthermore, it is noteworthy to highlight that almost all the numerical results presented in this study were specifically conducted for two coupled oscillators. Nonetheless, it is important to recognize that this adaptive blinking approach can be extended to encompass larger networks, irrespective of their network structure. The concept of adaptive coupling holds promise for further exploration in diverse scenarios, including identifying the most suitable variable for the coupling or incorporating weighted adaptive adjustments. This

suggests potential avenues for future research and applying adaptive coupling principles in various contexts.

ACKNOWLEDGMENTS

This work was partially funded by Centre for Nonlinear Systems, Chennai Institute of Technology, India, under Funding No. CIT/CNS/2023/RP/012.

AUTHOR DECLARATIONS

Conflict of Interest

The authors have no conflicts to disclose.

Author Contributions

Reza Irankhah: Investigation (equal); Software (equal); Writing – original draft (equal). **Mahtab Mehrabbeik:** Formal analysis (equal); Investigation (equal); Software (equal); Writing – original draft (equal). **Fatemeh Parastesh:** Formal analysis (equal); Funding acquisition (equal); Validation (equal); Writing – original draft (equal). **Karthikeyan Rajagopal:** Conceptualization (equal); Methodology (equal); Validation (equal); Writing – review & editing (equal). **Sajad Jafari:** Conceptualization (equal); Methodology (equal); Supervision (equal); Writing – review & editing (equal). **Jürgen Kurths:** Conceptualization (equal); Supervision (equal); Validation (equal); Writing – review & editing (equal).

DATA AVAILABILITY

Data sharing is not applicable to this article as no new data were created or analyzed in this study.

REFERENCES

- ¹S. Boccaletti, V. Latora, Y. Moreno, M. Chavez, and D. U. Hwang, “Complex networks: Structure and dynamics,” *Phys. Rep.* **424**, 175–308 (2006).
- ²F. Parastesh, S. Jafari, H. Azarnoush, Z. Shahriari, Z. Wang, S. Boccaletti, and M. Perc, “Chimeras,” *Phys. Rep.* **898**, 1–114 (2021).
- ³L. D. F. Costa, F. A. Rodrigues, G. Travieso, and P. R. Villas Boas, “Characterization of complex networks: A survey of measurements,” *Adv. Phys.* **56**, 167–242 (2007).
- ⁴S. Majhi, M. Perc, and D. Ghosh, “Dynamics on higher-order networks: A review,” *J. R. Soc., Interface* **19**, 20220043 (2022).
- ⁵S. M. Park and B. J. Kim, “Dynamic behaviors in directed networks,” *Phys. Rev. E* **74**, 026114 (2006).
- ⁶S.-W. Son, B. J. Kim, H. Hong, and H. Jeong, “Dynamics and directionality in complex networks,” *Phys. Rev. Lett.* **103**, 228702 (2009).
- ⁷M. Schirner, X. Kong, B. T. T. Yeo, G. Deco, and P. Ritter, “Dynamic primitives of brain network interaction,” *NeuroImage* **250**, 118928 (2022).
- ⁸L. A. N. Amaral and J. M. Ottino, “Complex networks,” *Eur. Phys. J. B* **38**, 147–162 (2004).
- ⁹H. Bao, Y. Zhang, W. Liu, and B. Bao, “Memristor synapse-coupled memristive neuron network: Synchronization transition and occurrence of chimera,” *Nonlinear Dyn.* **100**, 937–950 (2020).
- ¹⁰K. Li, B. Bao, J. Ma, M. Chen, and H. Bao, “Synchronization transitions in a discrete memristor-coupled bi-neuron model,” *Chaos, Solitons Fractals* **165**, 112861 (2022).
- ¹¹S. Rakshit, S. Majhi, J. Kurths, and D. Ghosh, “Neuronal synchronization in long-range time-varying networks,” *Chaos* **31**, 073129 (2021).
- ¹²A. Arenas, A. Díaz-Guilera, J. Kurths, Y. Moreno, and C. Zhou, “Synchronization in complex networks,” *Phys. Rep.* **469**, 93–153 (2008).

- ¹³S. Mirzaei, M. S. Anwar, F. Parastesh, S. Jafari, and D. Ghosh, “Synchronization in repulsively coupled oscillators,” *Phys. Rev. E* **107**, 014201 (2023).
- ¹⁴M. C. Romano, M. Thiel, and J. Kurths, “Generalized synchronization indices based on recurrence in phase space,” *AIP Conf. Proc.* **742**, 330–336 (2004).
- ¹⁵J. Kurths, M. C. Romano, M. Thiel, G. V. Osipov, M. V. Ivanchenko, I. Z. Kiss, and J. L. Hudson, “Synchronization analysis of coupled noncoherent oscillators,” *Nonlinear Dyn.* **44**, 135–149 (2006).
- ¹⁶E. M. Shahverdiev, S. Sivaprakasam, and K. A. Shore, “Lag synchronization in time-delayed systems,” *Phys. Lett. A* **292**, 320–324 (2002).
- ¹⁷V. N. Belykh, G. V. Osipov, V. S. Petrov, J. A. K. Suykens, and J. Vandewalle, “Cluster synchronization in oscillatory networks,” *Chaos* **18**, 037106 (2008).
- ¹⁸T. Wu, X. Zhang, and Z. Liu, “Understanding the mechanisms of brain functions from the angle of synchronization and complex network,” *Front. Phys.* **17**, 31504 (2022).
- ¹⁹F. A. S. Ferrari, R. L. Viana, A. S. Reis, K. C. Iarosz, I. L. Caldas, and A. M. Batista, “A network of networks model to study phase synchronization using structural connection matrix of human brain,” *Physica A* **496**, 162–170 (2018).
- ²⁰J. Bieler, R. Cannavo, K. Gustafson, C. Gobet, D. Gatfield, and F. Naef, “Robust synchronization of coupled circadian and cell cycle oscillators in single mammalian cells,” *Mol. Syst. Biol.* **10**, 739 (2014).
- ²¹F. A. D. S. Silva, S. R. Lopes, and R. L. Viana, “Synchronization of biological clock cells with a coupling mediated by the local concentration of a diffusing substance,” *Commun. Nonlinear Sci. Numer. Simul.* **35**, 37–52 (2016).
- ²²C. H. Totz, S. Olmi, and E. Schöll, “Control of synchronization in two-layer power grids,” *Phys. Rev. E* **102**, 022311 (2020).
- ²³M. Vlasceanu, M. J. Morais, and A. Coman, “Network structure impacts the synchronization of collective beliefs,” *J. Cognit. Cult.* **21**, 431–448 (2021).
- ²⁴I. Belykh, E. de Lange, and M. Hasler, “Synchronization of bursting neurons: What matters in the network topology,” *Phys. Rev. Lett.* **94**, 188101 (2005).
- ²⁵X. F. Wang and G. Chen, “Complex networks: Small-world, scale-free and beyond,” *IEEE Circuits Syst. Mag.* **3**, 6–20 (2003).
- ²⁶H. Hong, M. Y. Choi, and B. J. Kim, “Synchronization on small-world networks,” *Phys. Rev. E* **65**, 026139 (2002).
- ²⁷Y. Wu, Y. Shang, M. Chen, C. Zhou, and J. Kurths, “Synchronization in small-world networks,” *Chaos* **18**, 037111 (2008).
- ²⁸X. F. Wang and G. Chen, “Synchronization in scale-free dynamical networks: Robustness and fragility,” *IEEE Trans. Circuits Syst. I* **49**, 54–62 (2002).
- ²⁹Y. Moreno and A. F. Pacheco, “Synchronization of Kuramoto oscillators in scale-free networks,” *Europhys. Lett.* **68**, 603 (2004).
- ³⁰X. Wang, Y.-C. Lai, and C. H. Lai, “Enhancing synchronization based on complex gradient networks,” *Phys. Rev. E* **75**, 056205 (2007).
- ³¹M. Chavez, D. U. Hwang, A. Amann, H. G. E. Hentschel, and S. Boccaletti, “Synchronization is enhanced in weighted complex networks,” *Phys. Rev. Lett.* **94**, 218701 (2005).
- ³²S. Martineau, T. Saffold, T. T. Chang, and H. Ronellenfisch, “Enhancing synchronization by optimal correlated noise,” *Phys. Rev. Lett.* **128**, 098301 (2022).
- ³³A. E. Motter, C. S. Zhou, and J. Kurths, “Enhancing complex-network synchronization,” *Europhys. Lett.* **69**, 334 (2005).
- ³⁴A. E. Motter, C. Zhou, and J. Kurths, “Network synchronization, diffusion, and the paradox of heterogeneity,” *Phys. Rev. E* **71**, 016116 (2005).
- ³⁵A. Zeng, S.-W. Son, C. H. Yeung, Y. Fan, and Z. Di, “Enhancing synchronization by directionality in complex networks,” *Phys. Rev. E* **83**, 045101 (2011).
- ³⁶C. Zhou and J. Kurths, “Dynamical weights and enhanced synchronization in adaptive complex networks,” *Phys. Rev. Lett.* **96**, 164102 (2006).
- ³⁷S. Assenza, R. Gutiérrez, J. Gómez-Gardeñes, V. Latora, and S. Boccaletti, “Emergence of structural patterns out of synchronization in networks with competitive interactions,” *Sci. Rep.* **1**, 99 (2011).
- ³⁸Y.-H. Eom, S. Boccaletti, and G. Caldarelli, “Concurrent enhancement of percolation and synchronization in adaptive networks,” *Sci. Rep.* **6**, 27111 (2016).
- ³⁹J. Sawicki, R. Berner, S. A. M. Loos, M. Anvari, R. Bader, W. Barfuss, N. Botta, N. Bredé, I. Franović, D. J. Gauthier, S. Goldt, A. Hajizadeh, P. Hövel, O. Karin, P. Lorenz-Spreen, C. Miehl, J. Mölter, S. Olmi, E. Schöll, A. Seif, P. A. Tass, G. Volpe, S. Yanchuk, and J. Kurths, “Perspectives on adaptive dynamical systems,” *Chaos* **33**, 071501 (2023).
- ⁴⁰R. Berner, T. Gross, C. Kuehn, J. Kurths, and S. Yanchuk, “Adaptive dynamical networks,” *Phys. Rep.* **1031**, 1–59 (2023).

- ⁴¹F. Parastesh, K. Rajagopal, S. Jafari, M. Perc, and E. Schöll, “Blinking coupling enhances network synchronization,” *Phys. Rev. E* **105**, 054304 (2022).
- ⁴²Z. Dayani, F. Parastesh, F. Nazarimehr, K. Rajagopal, S. Jafari, E. Schöll, and J. Kurths, “Optimal time-varying coupling function can enhance synchronization in complex networks,” *Chaos* **33**, 033139 (2023).
- ⁴³L. Huang, Q. Chen, Y.-C. Lai, and L. M. Pecora, “Generic behavior of master-stability functions in coupled nonlinear dynamical systems,” *Phys. Rev. E* **80**, 036204 (2009).
- ⁴⁴L. M. Pecora and T. L. Carroll, “Master stability functions for synchronized coupled systems,” *Phys. Rev. Lett.* **80**, 2109–2112 (1998).
- ⁴⁵E. N. Lorenz, “Deterministic nonperiodic flow,” *J. Atmos. Sci.* **20**, 130–141 (1963).
- ⁴⁶O. E. Rössler, “An equation for continuous chaos,” *Phys. Lett. A* **57**, 397–398 (1976).
- ⁴⁷G. Chen and T. Ueta, “Yet another chaotic attractor,” *Int. J. Bifurcat. Chaos* **09**, 1465–1466 (1999).
- ⁴⁸J. L. Hindmarsh and R. M. Rose, “A model of neuronal bursting using three coupled first order differential equations,” *Proc. R. Soc. London B* **221**, 87–102 (1984).
- ⁴⁹A. Stefański, P. Perlikowski, and T. Kapitaniak, “Ragged synchronizability of coupled oscillators,” *Phys. Rev. E* **75**, 016210 (2007).
- ⁵⁰R. Mettin, U. Parlitz, and W. Lauterborn, “Bifurcation structure of the driven van der Pol oscillator,” *Int. J. Bifurcat. Chaos* **03**, 1529–1555 (1993).
- ⁵¹D. J. Watts and S. H. Strogatz, “Collective dynamics of ‘small-world’ networks,” *Nature* **393**, 440–442 (1998).
- ⁵²Z. Hagos, T. Stankovski, J. Newman, T. Pereira, P. V. E. McClintock, and A. Stefanovska, “Synchronization transitions caused by time-varying coupling functions,” *Phil. Trans. R. Soc. A* **377**, 20190275 (2019).
- ⁵³T. Stankovski, “Time-varying coupling functions: Dynamical inference and cause of synchronization transitions,” *Phys. Rev. E* **95**, 022206 (2017).
- ⁵⁴T. Stankovski, T. Pereira, P. V. E. McClintock, and A. Stefanovska, “Coupling functions: Universal insights into dynamical interaction mechanisms,” *Rev. Mod. Phys.* **89**, 045001 (2017).
- ⁵⁵Z. Li, L. Jiao, and J.-J. Lee, “Robust adaptive global synchronization of complex dynamical networks by adjusting time-varying coupling strength,” *Physica A* **387**, 1369–1380 (2008).
- ⁵⁶V. K. Chandrasekar, J. H. Sheeba, B. Subash, M. Lakshmanan, and J. Kurths, “Adaptive coupling induced multi-stable states in complex networks,” *Physica D* **267**, 36–48 (2014).
- ⁵⁷Q. Ren and J. Zhao, “Adaptive coupling and enhanced synchronization in coupled phase oscillators,” *Phys. Rev. E* **76**, 016207 (2007).
- ⁵⁸H. Bao, K. Rong, M. Chen, X. Zhang, and B. Bao, “Multistability and synchronization of discrete maps via memristive coupling,” *Chaos Solitons Fractals* **174**, 113844 (2023).
- ⁵⁹M. Chen, X. Luo, Y. Zhang, H. Wu, Q. Xu, and B. Bao, “Initial-boosted behaviors and synchronization of memristor-coupled memristive systems,” in *IEEE Transactions Circuits Systems I: Regular Papers* (IEEE, 2023), pp. 1–13.
- ⁶⁰P. R. Protachevich, K. C. Iarosz, I. L. Caldas, C. G. Antonopoulos, A. M. Batista, and J. Kurths, “Influence of autapses on synchronization in neural networks with chemical synapses,” *Front. Syst. Neurosci.* **14**, 604563 (2020).